Real-Time Emulation of a Hydrogen-Production Process for Assessment of an Active Wind-Energy Conversion System

Tao Zhou, Bruno Francois, *Senior Member, IEEE*, Mohamed el Hadi Lebbal, and Stéphane Lecoeuche, *Senior Member, IEEE*

***Abstract*—This paper presents the real-time emulation of a hydrogen-production process for assessment of an active wind-energy conversion system. The hardware-in-the-loop emulator of the electrolyzer consists of a power-electronic stage and a control stage. In the control board, the algorithmic equations of the electrolyzer modeling and its control should be implemented, as well as the emulator's power converter control. The causal ordering graph is used to model the electrolyzer and its auxiliary equipment. This model is capable of characterizing the relations among the different physical quantities and can be used to design the control system, ensuring an efficient and reliable operation of the electrolyzer. The proposed control method can manage the power and hydrogen flows. The simulation results have highlighted the variation domains and the relations among different physical quantities. The experimental results of the real-time emulation is based on a PHOEBUS advanced alkaline electrolyzer and shows the same electrical characteristics in real time with hardware.**

***Index Terms*—Electrolyzer, hybrid power systems (HPSs), hydrogen production, real-time simulation.**

I. Introduction

THE ADVANCING wind-power technologies have increased the use of wind-energy conversion systems (WECSs) for distributed generation to satisfy the grid energy demand [1]–[6]. However, the WECS, depending entirely on the wind generators, is a passive generator, which cannot offer any service to the grid, since the wind is an intermittent energy source. As solutions, hybrid power systems (HPSs) are proposed to overcome the problems with two innovative improvements.

1) *Storage subsystems* are associated with the wind generator to compensate or absorb the difference between the generated wind power and the required grid power [7]–[12].
2) *Energy management strategies* are needed to drive the power flows among the wind generator, the storage subsystems, and the grid. It has to implement various additional control functions to provide auxiliary services for the grid [10]–[12].

Thus, the wind-based HPS can offer some services to the grid and becomes an active WECS.

In our wind-based HPS (Fig. 1), supercapacitors are used for fast-dynamic energy storage, and the hydrogen technologies are used for long-term energy storage [13], [14]. These different energy conversion sources are connected to a common dc bus, and some energy management strategies are implemented in the control system, for satisfying the grid requirements while maximizing the benefit of renewable-energy sources and optimizing the operation of each storage unit. For example, the power management strategies for a normal operation are as follows.

1) The WECS works with a maximum power point tracking strategy. Therefore, the power generated from the wind generator P_{wg} is very fluctuant and not satisfactory to the required grid power P_{gc}.
2) To overcome this problem, the difference between the measured wind power and the grid power reference is used as a power reference for the storage units $(P_{\mathrm{sto\_ref}} = P_{\mathrm{wg\_mes}} - P_{\mathrm{gc\_ref}})$.
3) Since the fuel cell and the electrolyzer have relative slow dynamics, the slope of their power reference should be limited $(P_{\mathrm{H2\_ref}} \approx P_{\mathrm{sto\_ref}})$.
4) When $P_{\mathrm{H2\_ref}}$ is positive, the electrolyzer is activated to absorb the excess power $(P_{\mathrm{el\_ref}} = P_{\mathrm{H2\_ref}})$ and to produce the hydrogen, which is stored in the hydrogen tank for future use. When $P_{\mathrm{H2\_ref}}$ is negative, the fuel cell is activated to compensate the needed power $(P_{\mathrm{fc\_ref}} = |P_{\mathrm{H2\_ref}}|)$ by using the stored hydrogen. Thus, the fuel cell and the electrolyzer will never work at the same time.
5) During their transients, the supercapacitors are activated to compensate or absorb the difference between the power reference of the storage units and the measured power from the fuel cell/electrolyzer $(P_{\mathrm{sc\_ref}} = P_{\mathrm{sto\_ref}} - P_{\mathrm{fc\_mes}} + P_{\mathrm{el\_mes}})$.

Therefore, we can see that the long-term energy storage is performed in the form of hydrogen storage, through fuel cell and electrolyzer.

In order to achieve the required performances of the system and its control, a test bench has been built.

Manuscript received February 26, 2008; revised September 10, 2008. First published October 31, 2008; current version published February 27, 2009. This work was supported in part by the French National Agency of the Research (ANR SuperEner Project) and in part by the China Scholarship Council (CSC).

T. Zhou and B. Francois are with Laboratoire d'Electrotechnique et d'Electronique de Puissance, Ecole Centrale de Lille, Cité Scientifique, 59651 Villeneuve d'Ascq, France (e-mail: tao.zhou@ec-lille.fr; bruno.francois@ec-lille.fr).

M. el Hadi Lebbal and S. Lecoeuche are with the Department of Informatics and Control Systems, Ecole des Mines de Douai, 59508 Douai, France (e-mail: lebbal@ensm-douai.fr; lecoeuche@ensm-douai.fr).

Color versions of one or more of the figures in this paper are available online at http://ieeexplore.ieee.org.

Digital Object Identifier 10.1109/TIE.2008.2007048

0278-0046/$25.00 © 2009 IEEE

Authorized licensed use limited to: USTL. Downloaded on March 3, 2009 at 03:22 from IEEE Xplore. Restrictions apply.

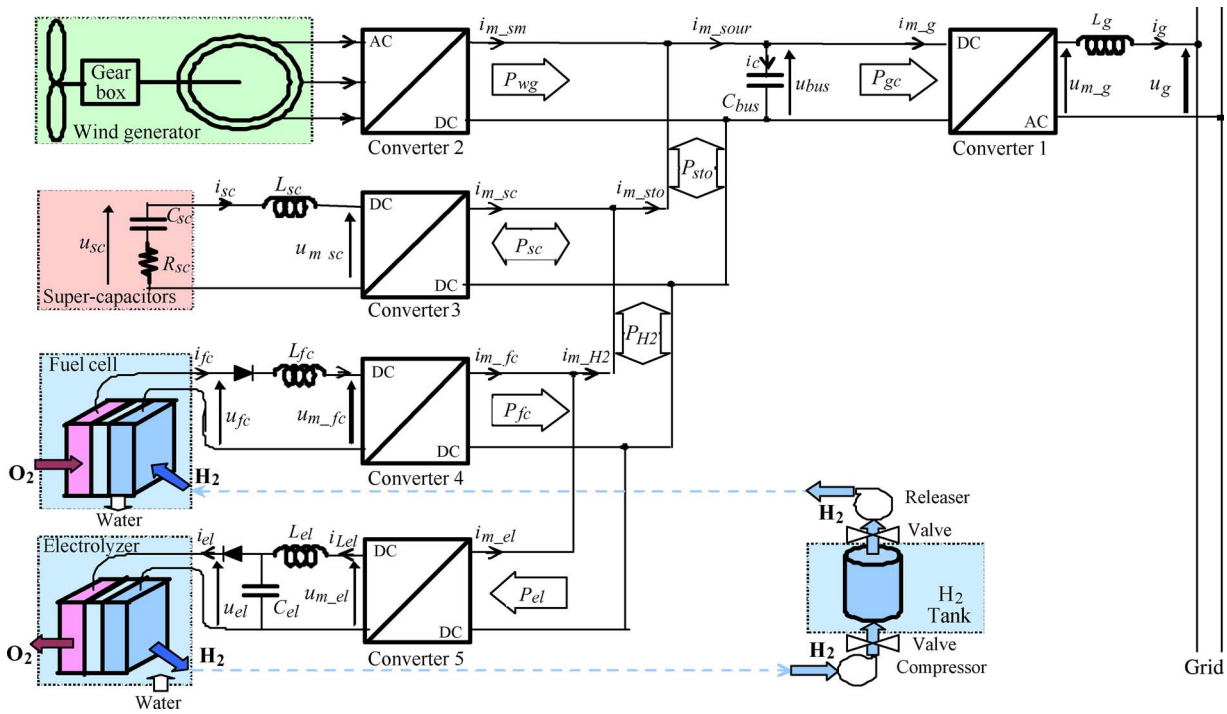

Fig. 1. Studied HPS based on wind-energy and hydrogen technologies.

Hardware-In-the-Loop (HIL) emulations of a part of a power system enable a fast experimental validation test before implementation with the real process. Some parts of the process are simulated in real time in a controller board and, then, are interfaced in hardware with the real devices. Such HIL simulation has been intensively used and enables to check availability and reliability of the storage units (component sizing, power-electronics interface, and operation control). We used this method to realize an electrolyzer emulator in order to test the assessment of the active WECS described earlier. Such an emulator can also be used to test and compare the electrical behaviors of different electrolyzer technologies. It consists of two parts: the power electronic stage, which is used to offer and emulate the electrolyzer's power; and the control stage, which is used for power-electronic device's control and electrolyzer's behavior emulation.

Therefore, the control stage is an important part, which determines the whole emulator's behavior.

Much research has been performed to model fuel cells, but the modeling of the electrolyzer has not yet been studied as widely as the fuel cell in the literature. In [15], the authors have developed a model for the unipolar Stuart cell electrolyzer, by assuming a fixed temperature and a 100% current efficiency, which has also been used in [16] and [17]. The higher heating value of the H_2 has also been used to give the theoretical model of the electrolysis process [18], [19]. Much more electrolyzer current–voltage characteristics are obtained empirically by experimental measurements and show much dependence on pressure and temperature. Some of these empirical models use the "log" term [20], [21] to describe the nonlinear relations between the voltage and current, while others use the "ln" term [22]–[25]. Some models have also been modified for the ease of control and simulation purposes [26], [27]. Electrolyzer models are generally formulated with the Faraday's Law, and the hydrogen-production rate depends proportionally on the current. However, detailed relations and causality among the physical quantities in the hydrogen-production system should be shown more clearly. The organization of the modeling equations should be suitable for an accurate dynamic simulation, for the control design, and for the power-management design together with the hydrogen-production subsystem, including power-conditioning system and hydrogen-gas-handling system.

In this paper, we focus on the hydrogen-production system to explain how the electrolyzer absorbs the electrical energy and converts it into hydrogen. A detailed control-oriented model is given by using a causal-ordering graph (COG) for the electrolyzer, as well as for the other parts for the hydrogen-production process. The model characterizes the relations among the different physical quantities and can be used to determine the control system ensuring efficient and reliable operation of the electrolyzer. This paper is organized as follows. The mathematical modeling of each part of the hydrogen-production process is presented in Section II, with dc–dc converter, electrolyzer, compressor, and hydrogen tank. In Section III, the control schemes are presented to manage the power flow and the hydrogen flow. The simulation results are presented in Section IV, and the relations among the different physical quantities are highlighted. A HIL emulator based on a real electrolyzer is presented in Section V to validate the modeling method, and the conclusions are given in Section VI.

II. Modeling of the Hydrogen-Production Process

In this section, the COG is used to model the electrolyzer and its auxiliary equipment. To simplify the modeling, the gas

Authorized licensed use limited to: USTL. Downloaded on March 3, 2009 at 03:22 from IEEE Xplore. Restrictions apply.

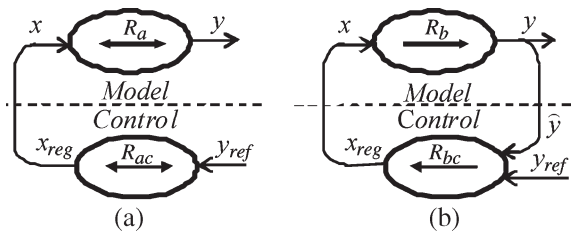

Fig. 2. COG of static and dynamic relations with their control schemes. (a) Static relation. (b) Dynamic relation.

is assumed to be dried and purified; all kinds of hydrogen leakage are assumed to be very small and can be neglected in the production, handling, and storage processes. The power-conditioning unit is performed by a power electronic converter. The gas-handling system can be modeled by a compressor, it supplies the necessary power to press the dry and purified hydrogen into the tank.

A. Presentation of the COG

The COG is a graphical representation of mathematical equations, which can be used to model a system and to design its control structure [28], [29]. Balloons with inside the equation number represent modeling relations. A static instantaneous relation has no time dependence. It will be depicted as a balloon with a bidirectional arrow, as shown in Fig. 2(a). Physically, it can be said that the corresponding element has an external causality orientation. If the variable x is externally set, it is then the input, and we get

$$R_a : y(t) = R_a\left(x(t)\right).$$

To make the output y equal to a reference $y_{\rm ref}$, an elementary control equation R_{ac}, obtained by inverting the modeling equation R_a to calculate the desired input variable $x_{\rm reg}$ from the reference $y_{\rm ref}$

$$R_{ac} : x_{\rm reg}(t) = R_{ac}\left(y_{\rm ref}(t)\right).$$

A time-dependent relation will be characterized by a unidirectional arrow in the balloon. Classically, dynamical systems are mathematically modeled by differential equations

$$\frac{dy(t)}{dt} = ax(t) + b.$$

This first-order differential equation is typically a time-dependent relation, whose output is formed by integration. It is represented by (R_b) in Fig. 2(b)

$$R_b : y(t) = R_b\left(x(t), t\right).$$

Moreover, the mathematical property of differential equations specifies that this equation type has an input–output orientation. Meanwhile, for equation R_b, the variable $x(t)$ must be the input and $y(t)$ must be the output. Physically, it can be said that the element has an internal causality orientation. The pure inverse equation introduces large instabilities due to the differential term. Instead of inverting R_b, we can use a closed-loop control

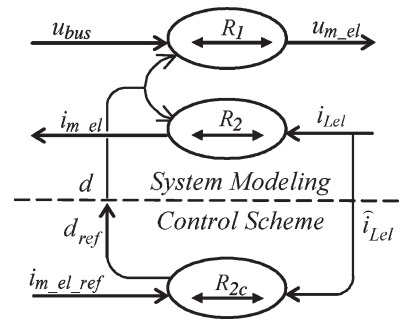

Fig. 3. COG of the buck converter and the power flow control.

with a corrector C_m to compensate the error signal between the measured output $\widehat{y}$ and the reference $y_{\rm ref}$

$$R_{bc} : x_{\rm reg}(t) = C_m\left(y_{\rm ref}(t) - \widehat{y}(t)\right).$$

B. Modeling of the Buck Converter

Since the voltage applied to the electrolyzer is smaller than the dc-bus voltage, a buck dc–dc converter is required between the dc bus and the electrolyzer to regulate the power transmitted to the electrolyzer. The average model of the buck converter is accurate enough to describe the process and can be used to simplify the system-modeling structure

$$R_1 : u_{\rm m\_el} = du_{\rm bus} \tag{1}$$

$$R_2 : i_{\rm m\_el} = di_{\rm Lel} \tag{2}$$

where $u_{\rm bus}$ and $i_{\rm m\_el}$ are, respectively, the dc-bus voltage and the modulated current of the buck converter, $u_{\rm m\_el}$ is the modulated voltage, and $i_{\rm Lel}$ is the inductor current. In steady state, the generated electrolyzer current $i_{\rm el}$ is equal to the inductor current $i_{\rm Lel}$. The duty cycle d is the control input. The corresponding COG of the converter is shown in Fig. 3.

C. Modeling of the Electrolyzer

The electrolyzer consumes the electrical power to produce hydrogen. Its modeling can be divided into four different parts: the electrical part, the electrochemical part, the thermal part, and the hydraulic part. The operation of the whole electrolyzer is based on the interaction among these four parts.

1) Electrical Part: Most reported models of electrolyzers' electrical behavior are obtained empirically by measurements [20]–[27]. Here, a well-adequate empirical model [20] is used to describe the characteristic of a given electrolyzer as shown in Fig. 4

$$R_3 : \begin{cases} u_{\rm cell} = u_0 + \frac{r_1 + r_2 T_{\rm el}}{A} i_{\rm el} + \left(s_1 + s_2 T_{\rm el} + s_3 T_{\rm el}^2\right) \\ \qquad \times \log\left(\frac{t_1 + t_2/T_{\rm el} + t_3/T_{\rm el}^2}{A} i_{\rm el} + 1\right) \\ u_{\rm el} = N_{\rm el} u_{\rm cell} \end{cases}. \tag{3}$$

In (3), $N_{\rm el}$ is the number of electrolyzer cells, $u_{\rm cell}$ is the voltage across one electrolyzer cell, $i_{\rm el}$ is the generated current of the electrolyzer, u_0 is the reversible cell voltage varying slowly

Authorized licensed use limited to: USTL. Downloaded on March 3, 2009 at 03:22 from IEEE Xplore. Restrictions apply.

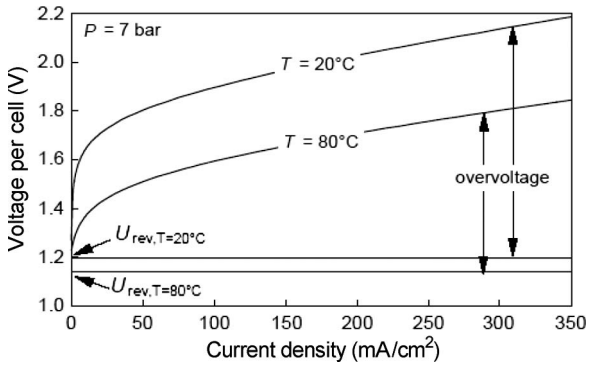

Fig. 4. Typical I–U characteristics of an electrolyzer cell (R_3) [20].

TABLE I
PARAMETERS OF THE ELECTROLYZER MODEL [20]

r_1	7.3e-5	Ω m^2	r_2	-1.1e-7	Ω m^2/°C
s_1	1.6e-1	V	s_2	1.38e-3	V/°C
s_3	-1.6e-5	V/°C^2	t_1	1.60e-2	m^2/A
t_2	-1.3	m^2 °C/A.	t_3	4.12e2	m^2 °C^2/A
A	0.25	m^2	a_1	99.5%	
a_2	-9.58	m^2/A	a_3	-0.056	m^2/A/°C
a_4	1502.7	m^4/A	a_5	-70.8	m^4/A/°C
N_{el}	21		T_{el}	25	°C

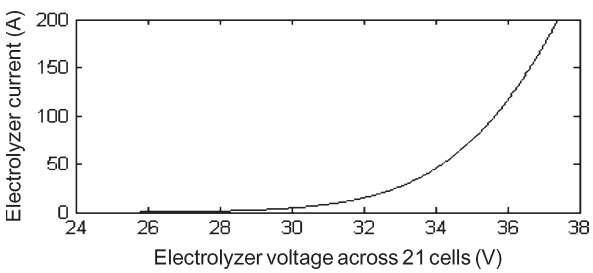

Fig. 5. Reciprocal relationship (R_3^{-1}) curve from $u_{\rm el}$ to $i_{\rm el}$ obtained by linear interpolation for a given $T_{\rm el} = 25$ °C.

with the temperature and pressure, r_i are the parameters for ohmic resistance of electrolyte, s_i and t_i are the parameters for overvoltage on electrodes, A is the area of the electrode, and $T_{\rm el}$ is the temperature of the electrolyte. All parameter values have been identified by measurements (Table I). This electrical characteristic depends mainly on voltage, current, and temperature. The nonlinear current versus voltage relationship shows that the electrolyzer can be considered as a variable nonlinear resistor. At a given temperature, the relationship between $u_{\rm el}$ and $i_{\rm el}$ is bijective (Fig. 4). The reciprocal relationship of the empirical model described in R_3 can be found by linear interpolation with a wished accuracy, as shown in Fig. 5. It is named R_3^{-1} and can be implemented in a lookup table. Thus, the current value $i_{\rm el}$ corresponding to each given voltage $u_{\rm el}$ can be easily obtained.

2) Electrical Part: The electrochemical reactions in water electrolysis can be summarized in Table II. According to the Faraday's law, the hydrogen-production rate $m'_{\rm el\_pro}$ depends on the electrolyzer current

$$R_4: \quad m'_{\rm el\_pro} = \alpha_{\rm el}(T_{\rm el}, i_{\rm el})\frac{N_{\rm el}}{nF} i_{\rm el} \tag{4}$$

where $N_{\rm el}$ is the number of electrolyzer cells, F is the Faraday constant, and n is the number of moles of transferred electrons per mole of water. The current efficiency $\alpha_{\rm el}$ varies also with the electrolyzer current density. The relation can be described by an empirical expression

$$\alpha_{\rm el} = a_1 \exp\left(\frac{a_2 + a_3 T}{i_{\rm el}/A} + \frac{a_4 + a_5 T}{(i_{\rm el}/A)^2}\right) \tag{5}$$

where the parameters $\alpha_i (i = 1, 2, \ldots, 5)$ are calculated from measurements and are given in Table I.

3) Thermal Part: The electrolyte temperature affects both the I–U curve and the Faraday efficiency. It can be determined by using simple (calculated from a quasi-static thermal model) or complex (calculated from a lumped thermal capacitance model) thermal models depending on the required accuracy. Since the time constant in the thermal domain is much larger than in the other physic domains, we suppose a constant temperature $T_{\rm el}$, which can be set externally, to substitute the thermal model.

4) Hydraulic Part: If we ignore the hydrogen leakage rate from the electrolyzer, the hydrogen evolution rate $m'_{\rm el}$ in the cathode depends on both the production rate $m'_{\rm el\_pro}$ and the outlet rate $m'_{\rm el\_out}$

$$R_5: m'_{\rm el}(\tau) = m'_{\rm el\_pro}(\tau) - m'_{\rm el\_out}(\tau). \tag{6}$$

The stored hydrogen quantity can be described as follows:

$$R_6: m_{\rm el}(t_0 + \Delta t) = \int_{t_0}^{t_0+\Delta t} m'_{\rm el}(\tau) d\tau + m_{\rm el}(t_0). \tag{7}$$

The hydrogen pressure in the electrolyzer can be found with the ideal gas law

$$R_7: p_{\rm el} = \frac{RT_{\rm el}}{V_{\rm el}} m_{\rm el} \tag{8}$$

where $p_{\rm el}$ and $T_{\rm el}$ are, respectively, the hydrogen pressure and temperature in the electrolyzer, R is the universal gas constant, and $V_{\rm el}$ is the volume of the cathode. In steady-state operation, the hydrogen outlet rate should be regulated to be equal to the hydrogen-production rate, and the stored hydrogen quantity in the cathode should be maintained constant as well as the pressure. The COG of the electrolyzer shows the organization of all modeling equations (Fig. 6).

D. Modeling of the Compressor

The compressor is based on a polytropic compression process. The relationship between the hydrogen molar flow rate (considered equal to the outlet rate from the electrolyzer $m'_{\rm el\_out}$) and the compressor power $P_{\rm comp}$ is

$$R_9: \quad m'_{\rm el\_out} = \frac{\alpha_{\rm comp}}{w} P_{\rm comp} \tag{9}$$

$$R_8: \quad w = \frac{kRT_{\rm el}}{k-1}\left[\left(\frac{p_{\rm sto}}{p_{\rm el}}\right)^{\frac{k-1}{k}} - 1\right] \tag{10}$$

where w is the polytropic work, $\alpha_{\rm comp}$ is the compressor efficiency, k is the polytropic coefficient, $T_{\rm el}$ is the inlet gas

Authorized licensed use limited to: USTL. Downloaded on March 3, 2009 at 03:22 from IEEE Xplore. Restrictions apply.

TABLE II
ELECTROCHEMICAL REACTIONS IN WATER ELECTROLYZERS

Electrolyte	Anode	Cathode
Alkaline (KOH)	$2OH^-(aq) \rightarrow \frac{1}{2}O_2(g)+H_2O+2e^-$	$2H_2O(l)+2e^- \rightarrow H_2(g)+2OH^-(aq)$
Acidic (SPE)	$H_2O(l) \rightarrow \frac{1}{2}O_2(g)+2H^+(aq)+2e^-$	$2H^+(aq)+2e^- \rightarrow H_2(g)$

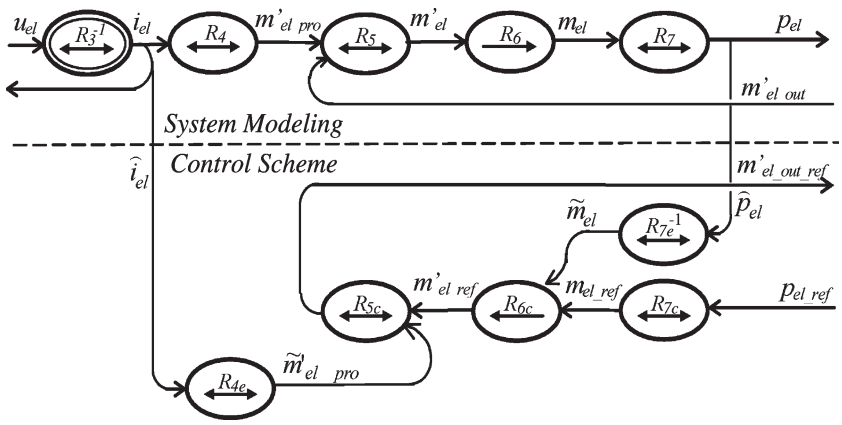

Fig. 6. COG of the electrolyzer and its pressure control.

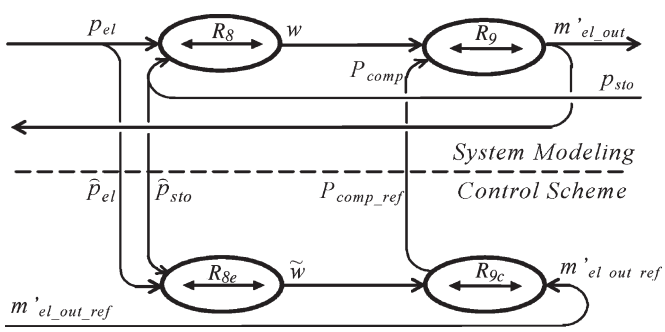

Fig. 7. COG of the compressor and the hydrogen flow control.

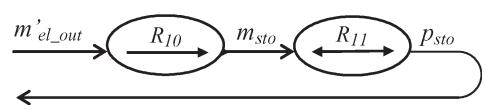

Fig. 8. COG of the hydrogen storage in production process.

temperature, $p_{\rm el}$ is the inlet gas pressure, corresponding to the hydrogen pressure in the electrolyzer, and $p_{\rm sto}$ is the outlet gas pressure, corresponding to the hydrogen pressure in the tank. The corresponding COG can be derived (Fig. 7).

E. Modeling of the Hydrogen Tank

The stored hydrogen rate $m'_{\rm sto}$ depends on three terms: the input flow rate $m'_{\rm el\_out}$ outlet from the electrolyzer, the outlet flow rate $m'_{\rm fc}$ to the fuel cell, and the leakage rate $m'_{\rm sto\_leak}$ to the environment

$$m'_{\rm sto}(\tau) = m'_{\rm el\_out}(\tau) - m'_{\rm fc}(\tau) - m'_{\rm sto\_leak}(\tau). \quad (11)$$

Since the electrolyzer and the fuel cell never work at the same time for efficiency reasons, the outlet flow rate is zero in the hydrogen-production process. If we neglect the leakage, the number of moles which are stored in the tank $m_{\rm sto}$ can be expressed as

$$R_{10}: \quad m_{\rm sto}(t_0+\Delta t) = \int_{t_0}^{t_0+\Delta t} m'_{\rm el}(\tau)d\tau + m_{\rm sto}(t_0). \quad (12)$$

The pressure in the hydrogen tank can be derived from the Van der Waals equation of state for real gases. However, for the ease of the modeling, we use the ideal gas law

$$R_{11}: \quad p_{\rm sto} = \frac{RT_{\rm sto}}{V_{\rm sto}} m_{\rm sto} \quad (13)$$

where $T_{\rm sto}$ is the gas temperature and $V_{\rm sto}$ is the storage-tank volume. Thus, the COG of the hydrogen tank is shown in Fig. 8.

F. Modeling of the Hydrogen-Production Process

We consider that the dc bus is equivalent to an ideal voltage source supplying a constant voltage $u_{\rm bus}$. Thus, the variation of the electrical power consumed by the electrolyzer $P_{\rm el}$ due to the intermittent wind energy can be expressed by the variation of the current $i_{\rm m\_el}$. Each COG model deduced earlier can be considered as a block with several inputs and outputs. If they are connected together by the corresponding inputs and outputs, a macroscopic representation of the hydrogen-production process can be obtained, as shown in Fig. 9. The blocks with a dotted line represent the parts where some time-dependent relation can be found and correspond to some process with energy accumulations. The temperatures, such as $T_{\rm el}$ and $T_{\rm sto}$, are assumed to be controlled by a thermostatic system. From the macrorepresentation, it is obviously shown that the duty ratio d and the compressor power $P_{\rm comp}$ are the control inputs, which can be used to regulate the transmitted power and the gas flow during the hydrogen-production process.

Authorized licensed use limited to: USTL. Downloaded on March 3, 2009 at 03:22 from IEEE Xplore. Restrictions apply.

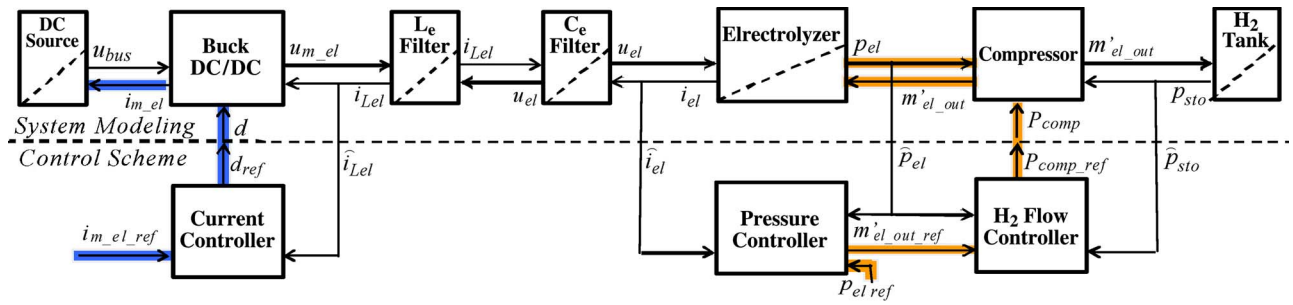

Fig. 9. Macroscopic representation of the system model with the control scheme of the hydrogen-production process.

III. Control of the Hydrogen-Production Process

A. General Principles

The design of the control system is based on the inversion of the COG model. The purposes of the control are to absorb the excess electrical power (which is produced by the wind generator) into hydrogen and to send the produced hydrogen gas toward the tank, by keeping the H_2 pressure constant in the electrolyzer for security and efficiency reasons. The whole control scheme consists of the following functions (Fig. 9):

1) a current controller, which guarantees the desired power flow by controlling the modulated current $i_{\mathrm{m\_el}}$ through the desired duty ratio d_{ref} of the buck converter;
2) an electrolyzer pressure controller, which maintains a constant H_2 pressure p_{el} in the electrolyzer by determining a desired H_2 outlet rate $m'_{\mathrm{el\_out\_ref}}$, which is equal to the H_2 production rate $m'_{\mathrm{el\_pro}}$ depending on the electrolyzer current i_{el};
3) a hydrogen flow controller, which drives the H_2 at the desired flow rate $m'_{\mathrm{el\_out\_ref}}$ by supplying the necessary compression power $P_{\mathrm{comp\_ref}}$.

B. Current Controller

Since the dc bus is considered as an ideal dc source with a constant voltage u_{bus}, the variation of the electrical power $P_{\mathrm{bus\_el}}$ transmitted to the electrolyzer can be expressed by the variation of the current $i_{\mathrm{m\_el}}$

$$\Delta P_{\mathrm{bus\_el}}(t) = u_{\mathrm{bus}} \Delta i_{\mathrm{m\_el}}(t). \tag{14}$$

Therefore, the power regulation can be performed by a current regulation. Since the relation (R_2) between the modulated current $i_{\mathrm{m\_el}}$ of the converter and the inductor current i_{Lel}, the current control algorithm can be given by inverting (R_2)

$$R_{2c}: \quad d_{\mathrm{ref}} = \frac{i_{\mathrm{m\_el\_ref}}}{\widehat{i}_{\mathrm{Lel}}} \tag{15}$$

where $\widehat{i}_{\mathrm{Lel}}$ is the sensed value of the current. The COG of the current control is shown in Fig. 3.

C. Pressure Controller

For a desired working condition, the H_2 pressure p_{el} should be set at a preferred level. Thus, the hydrogen outlet flow rate $m'_{\mathrm{el\_out}}$ from the electrolyzer should be equal to the hydrogen-production rate $m'_{\mathrm{el\_pro}}$ in the electrolyzer, in order to set a constant number of moles m_{el}, as well as the pressure p_{el} according to equation R_7. However, the molar flow rate cannot be easily measured. Since the constant pressure is the equivalent consequence of the H_2 flow rate control, we can try to make the reference outlet rate $m'_{\mathrm{el\_out\_ref}}$ to converge to the production rate $m'_{\mathrm{el\_ref}}$ in order to maintain the wished constant pressure $p_{\mathrm{el\_ref}}$.

By inverting equation R_7, the desired hydrogen number of moles $m_{\mathrm{el\_ref}}$ and the estimation of the number of moles $\tilde{m}_{\mathrm{el}}$ can be deduced directly from the reference pressure $p_{\mathrm{el\_ref}}$ and the measured pressure $\widehat{p}_{\mathrm{el}}$

$$R_{7c}: \quad m_{\mathrm{el\_ref}} = \frac{V_{\mathrm{el}}}{RT_{\mathrm{el}}} p_{\mathrm{el\_ref}} \tag{16}$$

$$R_{7e}: \quad \tilde{m}_{\mathrm{el}} = \frac{V_{\mathrm{el}}}{RT_{\mathrm{el}}} \widehat{p}_{\mathrm{el}}. \tag{17}$$

Then, the reference hydrogen variation rate $m'_{\mathrm{el\_ref}}$ in the electrolyzer can be obtained through a closed-loop control with a corrector C_m

$$R_{6c}: m'_{\mathrm{el\_ref}} = C_m(m_{\mathrm{el\_ref}} - \tilde{m}_{\mathrm{el}}). \tag{18}$$

The reference of the hydrogen outlet flow rate $m'_{\mathrm{el\_out\_ref}}$ from the electrolyzer can be obtained by inverting (R_5)

$$R_5^{-1}: \quad m'_{\mathrm{el\_out\_ref}} = \tilde{m}'_{\mathrm{el\_pro}} - m'_{\mathrm{el\_ref}}. \tag{19}$$

The estimated hydrogen-production rate $\tilde{m}'_{\mathrm{el\_pro}}$ is deduced directly from the sensed electrolyzer current $\widehat{i}_{\mathrm{el}}(R_4)$

$$R_{4e}: \quad \tilde{m}'_{\mathrm{el\_pro}} = \tilde{\alpha}_{\mathrm{el}}(T_{\mathrm{el}}, \widehat{i}_{\mathrm{el}}) \frac{N_{\mathrm{el}}}{nF} \widehat{i}_{\mathrm{el}} \tag{20}$$

where the estimated current efficiency $\tilde{\alpha}_{\mathrm{el}}$ can also be obtained from the sensed electrolyzer current $\widehat{i}_{\mathrm{el}}$

$$\tilde{\alpha}_{\mathrm{el}} = a_1 \exp\left(\frac{a_2 + a_3 T}{\widehat{i}_{\mathrm{el}}/A} + \frac{a_5 + a_6 T}{(\widehat{i}_{\mathrm{el}}/A)^2}\right). \tag{21}$$

The COG of the pressure control is shown in Fig. 6.

Authorized licensed use limited to: USTL. Downloaded on March 3, 2009 at 03:22 from IEEE Xplore. Restrictions apply.

D. Hydrogen Flow Controller

The role of the compressor is to drive the hydrogen to the tank at the reference outlet flow rate $m'_{\mathrm{el\_out\_ref}}$. The desired compressor power $P_{\mathrm{comp\_ref}}$ can be calculated by inverting (R_9)

$$R_{9c}: \quad P_{\mathrm{comp\_ref}} = \frac{\tilde{w}}{\alpha_{\mathrm{comp}}} m'_{\mathrm{el\_out\_ref}} \tag{22}$$

where the value of the polytropic work $\tilde{w}$ is estimated with the measured pressures $\widehat{p}_{\mathrm{sto}}$ and $\widehat{p}_{\mathrm{el}}$

$$R_{8e}: \quad \tilde{w} = \frac{kRT_{\mathrm{el}}}{k-1}\left[\left(\frac{\widehat{p}_{\mathrm{sto}}}{\widehat{p}_{\mathrm{el}}}\right)^{\frac{k-1}{k}} - 1\right]. \tag{23}$$

The COG of the hydrogen flow control is shown in Fig. 7.

E. Entire Control Scheme

When we gather all COGs together, the macroscopic representation of the whole system model with its entire control scheme can be obtained, as shown in Fig. 9.

IV. Simulation of the Hydrogen-Production Process

The model of this system is simulated with the presented control scheme in MATLAB/Simulink, with $u_{\mathrm{bus}} = 48$ V, $T_{\mathrm{el}} = 25$ °C, $V_{\mathrm{el}} = 1$ L, $V_{\mathrm{sto}} = 5$ L, and the initial pressures $p_{\mathrm{el}} = 3$ bar and $p_{\mathrm{sto}} = 20$ bar. The compressor efficiency is assumed to be equal to 63%. It is widely accepted that one of the main weak points of the electrolyzer is its time constant, which depends on the auxiliary systems. As it is well known, by omitting all the kinds of losses, the supplied power corresponds directly to the hydrogen-production rate. If the power variation is faster than the gas-delivery-control capacity, the hydrogen pressure in the electrolyzer can no longer be controlled, and some security problems will occur. Therefore, in practice, power slopes are always given for transients. Since the slope is limited much slower than the gas-handling dynamic, the static models of the electrolyzer and compressor are enough to show the behavior of the hydrogen-production process in this quasi-static working condition. In [30], an alkaline electrolyzer of 20 kW can increase its power from 16% to 100% of its normal power within 40 s, nearly 500 W/s. Moreover, in this paper, we give a power slope of 125 W/s, converted in current reference $i_{\mathrm{m\_el\_ref}}$ [Fig. 10(a)].

The time evolutions of the physical quantities and the relation among these quantities have been clearly shown in Fig. 10. The duty ratio d depends directly on the current reference $i_{\mathrm{m\_el\_ref}}$ through the control law [Fig. 10(b)]. The electrolyzer voltage u_{el} depends on such a varying duty ratio [Fig. 10(c)], since the dc-bus voltage u_{bus} is nearly constant. The electrolyzer current i_{el} depends on the electrolyzer voltage u_{el} according to electrolyzer model equations [Fig. 10(d)]. Since the hydrogen-production rate is proportional to the electrolyzer current through the Faraday law, the hydrogen outlet rate $m'_{\mathrm{el_out}}$ [Fig. 10(e)] is regulated and is equal to the hydrogen-production rate (in steady state) by the compressor power P_{comp} [Fig. 10(h)] in order to maintain the pressure p_{el} constant [Fig. 10(f)]. As a result, the hydrogen pressure p_{sto} [Fig. 10(g)] in the tank depends on the hydrogen outlet rate from the electrolyzer $m'_{\mathrm{el\_out}}$.

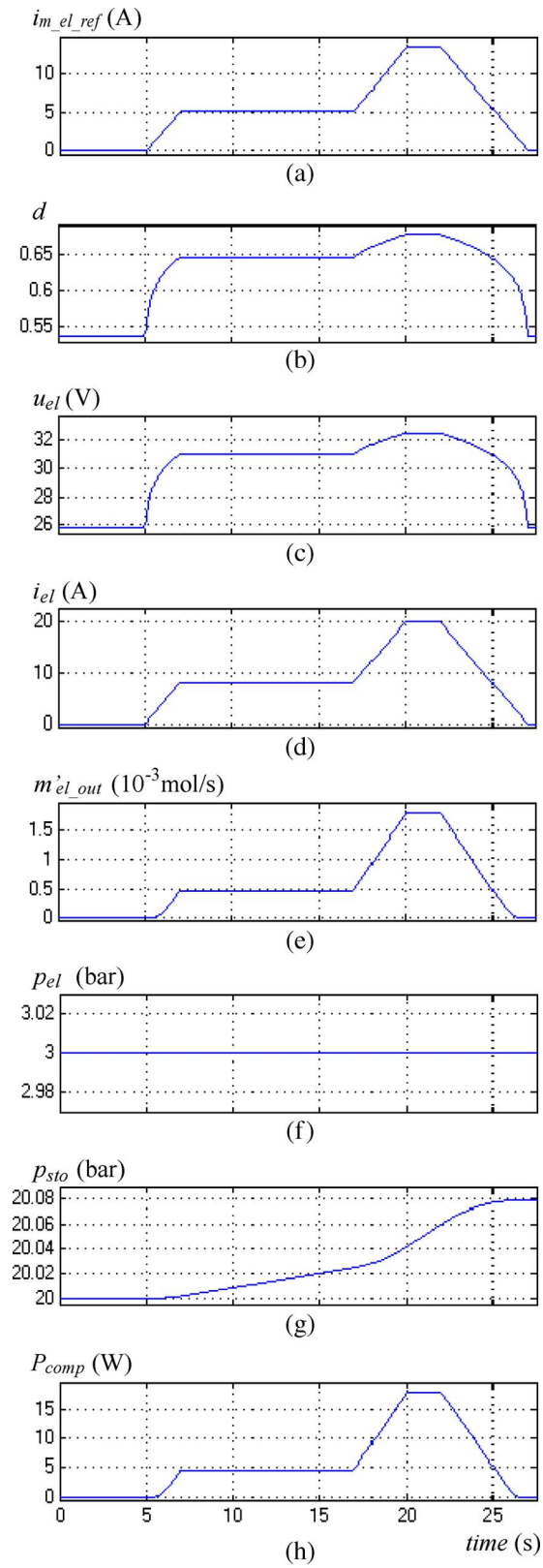

Fig. 10. Simulation results of the response to the power slope.

Authorized licensed use limited to: USTL. Downloaded on March 3, 2009 at 03:22 from IEEE Xplore. Restrictions apply.

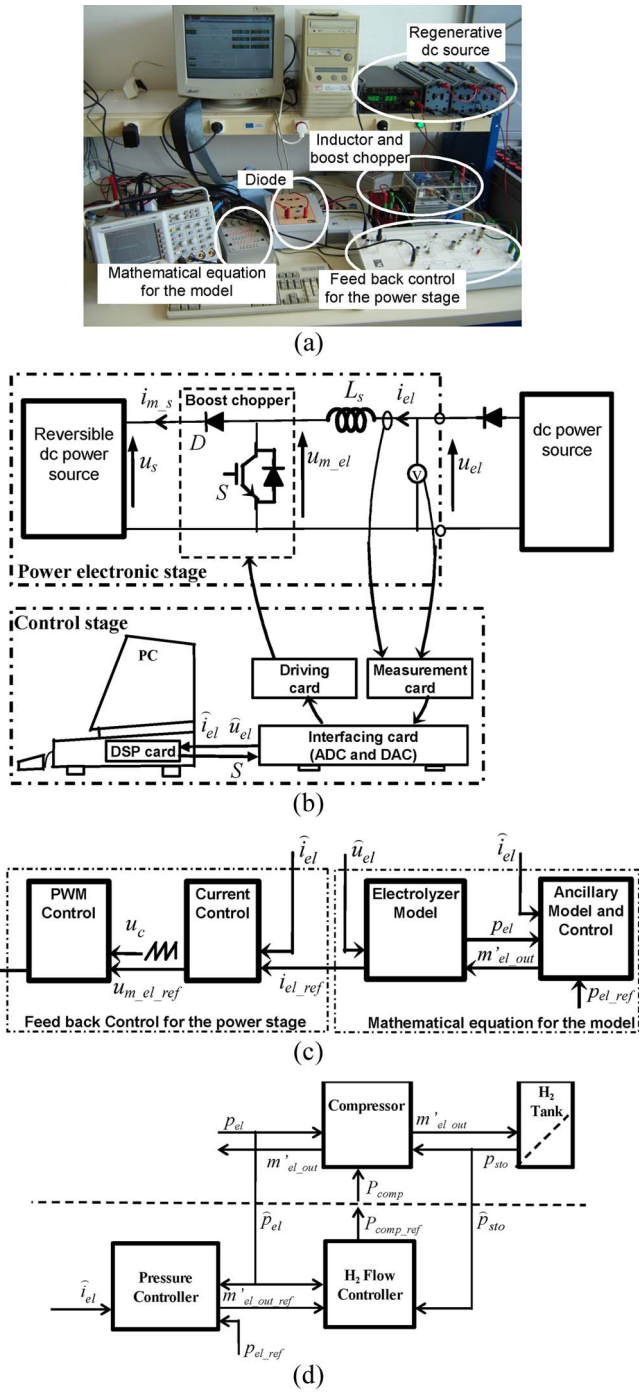

Fig. 11. Electrolyzer emulator's schematic diagraph. (a) HIL emulator of the electrolyzer. (b) Structure of the electrolyzer emulator. (c) Functional blocks implemented in the DSP card. (d) Contents of the auxiliary model and control block (part of Fig. 9).

V. HIL Emulator

A HIL emulator of the electrolyzer has been designed with experimental data from a PHOEBUS advanced alkaline electrolyzer [31]. The cells are circular and bipolar; they have a zero-spacing geometry; and they consist of NiO diaphragms and activated electrodes which make them highly efficient. It can offer in real time the same terminal electrical characteristics as a real electrolyzer and, so, is used to test the active WECS [Fig. 11(a)]. Such an electrolyzer emulator can enable the test

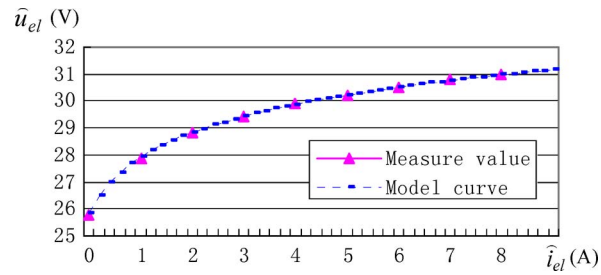

Fig. 12. Comparison of the emulator's sensed data with the electrolyzer's static characteristic.

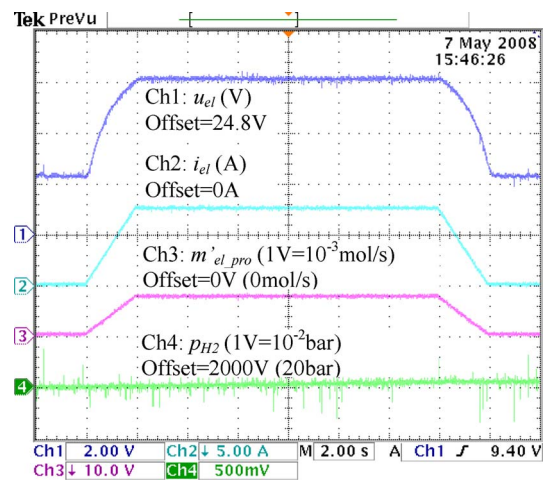

Fig. 13. Electrolyzer emulator's response to power slope.

and comparison of the different electrolyzer devices with their corresponding mathematical models given by the manufacturer. Moreover, for studying the power-management strategies of the HPS, it can be enough to use such an emulator instead of a real expensive electrolyzer.

The used electrolyzer emulator can be divided into two stages: the power-electronic stage and the control stage [Fig. 11(b)]. The power-electronic stage consists of a boost dc/dc converter with an ideal regenerative source. It is designed to set the same current i_{el} as for a real electrolyzer. The control stage consists of the chopper's driving card, the measurement instruments, the digital signal processing (DSP) card, and the interfacing card.

The software of the emulator is implemented in the DSP card [Fig. 11(c)]. A feedback closed loop is used to control the equivalent electrolyzer current i_{el}. The current reference $i_{\mathrm{el\_ref}}$ is calculated from the electrolyzer model and pressure controller parts (Fig. 9), with a given pressure reference and the sensed voltage value $\widehat{u}_{\mathrm{el}}$. The static electrical characteristic R_3^{-1} with 21 cells of 0.25 m^2 has been implemented with the same parameters as used in the simulation earlier. We can see that the obtained emulator's static characteristic corresponds well to the model curve (Fig. 12).

When we give the same power slope variation to the emulator as in the simulation (from $t = 0$ s to $t = 17$ s), the emulator can run in the quasi-static condition with the given temperature and pressure. The electrolyzer emulator's terminal response corresponds to the simulation results presented previously (Fig. 13).

Authorized licensed use limited to: USTL. Downloaded on March 3, 2009 at 03:22 from IEEE Xplore. Restrictions apply.

Different auxiliary system models and their control algorithms can also be implemented in the DSP card, according to different purposes and methods. For example, we can implement the auxiliary system's model described earlier [Fig. 11(d)] to establish the relation between the electrolyzer and the hydrogen storage. The variation of the different physical quantities can also be simulated in the DSP card and verified via the computer desk in real time (Fig. 13), such as the hydrogen outlet flow rate $m'_{\mathrm{H2\_out}}$ by using the computed equation R_3^{-1} and the hydrogen pressure p_{sto} in the storage by using the computed equations R_{10} and R_{11}, etc.

VI. Conclusion

First, a control-oriented modeling of an electrolyzer, as well as the auxiliary system for the hydrogen-production process has been presented by using a COG. The model is able to characterize the relations among the different physical quantities and can be used to determine the control system, ensuring efficient and reliable operation of the electrolyzer. The proposed control method can regulate the power flow and the hydrogen flow. With a slow power slope, the system can be considered quasi-static and the temperature can be considered constant, with external thermostatic system. We need to measure only a few quantity values to correct the two control inputs: the duty ratio d and the compressor power P_{comp}. The simulation results have highlighted the variation domains and dynamics of physical quantities.

Second, a HIL emulation of this hydrogen-production process has been presented. This real-time emulator is based on a PHOEBUS advanced alkaline electrolyzer. It consists of a power-electronic stage and a control stage. The power-electronic stage can offer the same electrical characteristics as the real electrolyzer, with the help of the power-converter-control algorithms and the modeling equations of the electrolyzer system implemented in the control board. Such an electrolyzer emulator can help to test assessment of an active WECS in the future.

References

[1] A. G. Abo-Khalil and D.-C. Lee, "MPPT control of wind generation systems based on estimated wind speed using SVR," *IEEE Trans. Ind. Electron.*, vol. 55, no. 3, pp. 1489–1490, Mar. 2008.

[2] A. Mirecki, X. Roboam, and F. Richardeau, "Architecture complexity and energy efficiency of small wind turbines," *IEEE Trans. Ind. Electron.*, vol. 54, no. 1, pp. 660–670, Feb. 2007.

[3] H. Geng, W. Zhou, and G. Yang, "Inverse-system control approach for variable-speed variable-pitch wind generator," in *Proc. IEEE IECON*, Nov. 5–8, 2007, pp. 1627–1632.

[4] T. H. Yeh and L. Wang, "A study on generator capacity for wind turbines under various tower heights and rated wind speeds using Weibull distribution," *IEEE Trans. Energy Convers.*, vol. 23, no. 2, pp. 592–602, Jun. 2008.

[5] F. Blaabjerg, R. Teodorescu, M. Liserre, and A. V. Timbus, "Overview of control and grid synchronization for distributed power generation systems," *IEEE Trans. Ind. Electron.*, vol. 53, no. 5, pp. 398–1409, Oct. 2006.

[6] J. M. Carrasco, L. G. Franquelo, J. T. Bialasiewicz, E. Galvan, R. C. Portillo Guisado, M. A. M. Prats, J. I. Leon, and N. Moreno-Alfonso, "Power-electronic systems for the grid integration of renewable energy sources: A survey," *IEEE Trans. Ind. Electron.*, vol. 53, no. 4, pp. 1002–1016, Jun. 2006.

[7] G. O. Cimuca, C. Saudemont, B. Robyns, and M. Radulescu, "Control and performance evaluation of a flywheel energy-storage system associated to a variable-speed wind generator," *IEEE Trans. Ind. Electron.*, vol. 53, no. 4, pp. 1074–1085, Jun. 2006.

[8] S. Lemofouet and A. Rufer, "A hybrid energy storage system based on compressed air and supercapacitors with Maximum Efficiency Point Tracking (MEPT)," *IEEE Trans. Ind. Electron.*, vol. 53, no. 4, pp. 1105–1115, Jun. 2006.

[9] C. Abbey and G. Joos, "Supercapacitor energy storage for wind energy applications," *IEEE Trans. Ind. Electron.*, vol. 43, no. 3, pp. 769–776, May 2007.

[10] J. Schonberger, R. Duke, and S. D. Round, "DC-bus signaling: A distributed control strategy for a hybrid renewable nanogrid," *IEEE Trans. Ind. Electron.*, vol. 53, no. 5, pp. 1453–1460, Oct. 2006.

[11] M. Tekin, D. Hissel, M. C. Pera, and J. M. Kauffmann, "Energy-management strategy for embedded fuel-cell systems using fuzzy logic," *IEEE Trans. Ind. Electron.*, vol. 54, no. 1, pp. 595–603, Feb. 2007.

[12] P. Thounthong, S. Rael, and B. Davat, "Control strategy of fuel cell and supercapacitors association for a distributed generation system," *IEEE Trans. Ind. Electron.*, vol. 54, no. 6, pp. 3225–3233, Dec. 2007.

[13] B. Francois, D. Hissel, and M. T. Iqbal, "Dynamic modelling of a fuel cell and wind turbine DC-linked power system," in *Proc. Electrimacs*, Hammamet, Tunisia, Apr. 17–20, 2005, CD-ROM.

[14] T. Zhou, B. Francois, M. Labbal, and S. Lecoeuche, "Modeling and control design of hydrogen production process by using a causal ordering graph for wind energy conversion system," in *Proc. IEEE ISIE*, Vigo, Spain, Jun. 2007, CD-ROM.

[15] K. Sapru *et al.*, "Development of a small scale hydrogen production-storage system of hydrogen applications," in *Proc. IECEC*, Jul. 27–Aug. 1, 1997, pp. 1947–1952.

[16] M. T. Iqbal, "Simulation of a small wind fuel cell hybrid energy system," *Renew. Energy*, vol. 28, no. 4, pp. 511–522, Apr. 2003.

[17] T. F. El-Shatter, M. N. Eskandar, and M. T. El-Hagry, "Hybrid PV/fuel cell system design and simulation," *Renew. Energy*, vol. 27, no. 3, pp. 479–485, Nov. 2002.

[18] J. Hamelin, K. Agbossou, A. Laperrière, F. Laurencelle, and T. K. Bose, "Dynamic behavior of a PEM fuel cell stack for stationary applications," *Hydrogen Energy*, vol. 26, no. 6, pp. 625–629, Jun. 2001.

[19] M. Korpas and A. T. Holen, "Operation planning of hydrogen storage connected to wind power operating in a power market," *IEEE Trans. Energy Convers.*, vol. 21, no. 3, pp. 742–749, Sep. 2006.

[20] Ø. Ulleberg, "Modeling of advanced alkaline electrolyzers: A system simulation approach," *Hydrogen Energy*, vol. 28, no. 1, pp. 21–33, Jan. 2003.

[21] C. Boccaletti, G. Di Grazia, G. Fabbri, and E. Nisticò, "Energy models for stand alone power systems," in *Proc. EETI*, Rio de Janeiro, Brazil, Oct. 2004.

[22] J. P. Vanhanen and P. D. Lund, "Computational approaches for improving seasonal storage systems based on hydrogen technologies," *Hydrogen Energy*, vol. 20, no. 7, pp. 575–585, Jul. 1995.

[23] K. Agbossou, M. Kolhe, J. Hamelin, and T. K. Bose, "Performance of a stand-alone renewable energy system based on energy storage as hydrogen," *IEEE Trans. Energy Convers.*, vol. 19, no. 3, pp. 633–640, Sep. 2004.

[24] Kélouwani, K. Agbossou, and R. Chahine, "Model for energy conversion in renewable energy system with hydrogen storage," *Power Sources*, vol. 140, no. 2, pp. 392–399, Feb. 2005.

[25] M. Santarelli and D. Pellegrino, "Mathematical optimization of a RES-H2 plant using a black box algorithm," *Renew. Energy*, vol. 30, no. 4, pp. 493–510, Apr. 2005.

[26] A. Bilodeau and K. Agbossou, "Control analysis of renewable energy system with hydrogen storage for residential applications," *J. Power Sources*, vol. 162, no. 2, pp. 757–764, Nov. 22, 2006.

[27] H. Görgün, "Dynamic modelling of a Proton Exchange Membrane (PEM) electrolyzer," *Hydrogen Energy*, vol. 31, no. 1, pp. 29–38, Jan. 2006.

[28] X. Guillaud, P. Degobert, and J. P. Hautier, "Modeling control and causality: The causal ordering graph," in *Proc. 16th IMACS Control Eng.*, Lausanne, Switzerland, 2000, CD-ROM.

[29] X. Guillaud and B. Francois, "A causal method for the modelling of static converter and the control design: Application to a voltage source converter," in *Proc. EPE*, Toulouse, France, Sep. 2003. CD.

[30] F. Menzl and M. Wenske, "Investigation of the steady state and transient operating behaviour of a 20 kW pressure electrolyser," in *Hydrogen Power: Theoretical and Engineering Solutions*, T. O. Saetre, Ed. Amsterdam, The Netherlands: Kluwer, 1998, pp. 185–190.

[31] Ø. Ulleberg, "Stand-alone power systems for the future: Optimal design, operation & control of solar–hydrogen energy systems," Ph.D. dissertation, Norwegian Univ. Sci. Technol., Trondheim, Norway, 1998.

Authorized licensed use limited to: USTL. Downloaded on March 3, 2009 at 03:22 from IEEE Xplore. Restrictions apply.

Tao Zhou was born in Shandong, China, in 1981. He received the M.S. degree in power electronics and power drives from Southwest Jiaotong University, Chengdu, China, in 2006, and the Engineering degree from the Ecole Centrale de Lyon, Lyon, France, in 2006. He is currently working toward the Ph.D. degree in electrical engineering in the Laboratoire d'Electrotechnique et d'Electronique de Puissance, Ecole Centrale de Lille, Villeneuve d'Ascq, France.

His main research interests include energy management and energy storage in distributed power-generation systems based on renewable-energy sources.

Bruno Francois (M'96–SM'06) was born in Saint Amand les Eaux, France, in 1969. He received the Ph.D. degree from the University of Lille, Lille, France, in 1996.

He is currently an Associate Professor with the Department of Electrical Engineering, Ecole Centrale de Lille, Villeneuve d'Ascq, France, where he is also a member of the Laboratoire d'Electrotechnique et d'Electronique de Puissance. He is currently working on renewable-energy-based active generators and the design of advanced energy-management systems.

Mohamed el Hadi Lebbal was born in Batna, Algeria, in 1975. He received the Ph.D. degree in automatic control from the University of Havre, Havre, France, in 2006.

He was with the Department of Informatics and Control Systems, Ecole des Mines de Douai, Douai, France, where he was working on the areas of fault detection and isolation control and modulation of renewable-energy-based power systems. He has been researching in these areas and teaches courses on automatic control at the University of Maine, Le Mans, France.

Stéphane Lecoeuche (M'98–SM'05) was born in Auchel, France, in 1970. He received the Ph.D. degree from the University of Lille, Lille, France, in 1998.

Since 2005, he has been a Professor with the Department of Informatics and Control Systems, Ecole des Mines de Douai, Douai, France. His research interests include system identification and dynamical learning applied to the modeling and monitoring of complex evolving systems.

Authorized licensed use limited to: USTL. Downloaded on March 3, 2009 at 03:22 from IEEE Xplore. Restrictions apply.